Chinese Chemical Letters 34 (2023) 107417

Contents lists available at ScienceDirect

Chinese Chemical Letters

journal homepage: www.elsevier.com/locate/cclet

Photocatalytic fuel cell for simultaneous antibiotic wastewater treatment and electricity production by anatase TiO_2 nanoparticles anchored on Ni foam

Jinhan Li[a], Xicheng Li[a], Shaobin Yu[a], Shuai Gao[c], Yang Zhang[b,*], Yan Li[a], Changzheng Wang[a,*], Qiang Wang[c,*]

[a] Beijing Key Laboratory of Functional Materials for Building Structure and Environment Remediation, Beijing University of Civil Engineering and Architecture, Beijing 100044, China
[b] College of Chemistry, Beijing Normal University, Beijing 100875, China
[c] Laboratory for Micro-sized Functional Materials & College of Elementary Education, Capital Normal University, Beijing 100048, China

ARTICLE INFO

Article history:
Received 7 November 2021
Revised 23 February 2022
Accepted 7 April 2022
Available online 11 April 2022

Keywords:
Photocatalytic fuel cell
TiO_2
Ni foam
Electricity production
Antibiotic wastewater treatment

ABSTRACT

Photocatalytic fuel cell (PFC) holds great potential for the sustainable production of electricity and degradation of organic pollutants for solving global energy and environmental problems. However, the efficient photodegradation of organic dyes and antibiotic drugs, such as ciprofloxacin (CIP) and methylene blue (MB), remains challenging. Aiming at improving the separation efficiency of hole and electron for electricity generation in the PFC system, TiO_2-NPs@NF-*x* photoanode was fabricated by a cost-effective and laborsaving hydrothermal approach. The as-fabricated photoanode demonstrated abundant active sites, enhanced light harvesting capacity and photogenerated charge carrier separation. At a CIP-HCl concentration of 10 mg/L and pH value of about 7, 85% of CIP-HCl can be efficiently removed after 3 h irradiation by 300 W Xe lamp. TiO_2-NPs@NF-20 photoelectrode based PFC system exhibited an impressed ability to simultaneously degrade ciprofloxacin and generate electricity under light irradiation with an open circuit voltage of 1.021 V, short circuit current density and maximum power density of 2.4 mA/cm^2, 0.357 mW/cm^2, respectively. This work provided a cost-effective method for the treatment of organic waste and generation of electrical power.

Currently, worldwide freshwater crisis is one of the most serious social problems. Recycling and reusing urban wastewater have been developed as a sustainable approach to meet the increasing demand for fresh and safe water source. Since the rapid population growth, industrialization and urbanization over the last half century, massive organic pollutants were continually discharged into surface water and groundwater [1]. However, conventional wastewater treatment processes are not designed to degrade and/or remove organic pollutants, such as organic dyes and antibiotics. Recently, antibiotics are extensively detected in urban ecosystems due to the huge consumption and excretion from human and animal waste (*e.g.*, urine and feces). Although the antibiotic residues are found at a low concentration in aquatic ecosystems, it can be bioaccumulated through the food chains due to their resistant to biodegradation by microorganisms, which became a serious threat to public health. Unfortunately, the misuse and/or overuse of antibiotics led to antibiotic resistance in common bacteria [2]. Therefore, it is crucial to develop a cost-effective approach to eliminate antibiotic in urban wastewater. As a broad-spectrum fluoroquinolone antibiotic, ciprofloxacin (CIP) is extensively used in the therapy of urinary and respiratory tract infections [3,4]. However, CIP cannot be completely metabolized and absorbed by human or animal while more than 75% of the residues is found to be mainly excreted through the feces and urine, and eventually discarded into municipal sewage [5]. CIP has been identified as one of the major pharmaceutical contaminants in the water cycle [6] and listed as a key priority pollutant by European Union [7]. Due to their persistence, they tend to bioaccumulate along the food chain and affect ecosystem functions [8]. The negative effects of CIP on organisms include antibiotic resistance in microorganisms, especially in *Enterococci* and *Escherichia coli*, which can mutate and even develop resistance [9]. Furthermore, CIP is also known to bioaccumulate, which is found to be one of the most frequently detected antibiotics in fish muscle tissue from the Haihe River in China [10].

* Corresponding authors.
E-mail addresses: y.zhang@bnu.edu.cn (Y. Zhang), changzhwang@163.com (C. Wang), qwchem@gmail.com (Q. Wang).

https://doi.org/10.1016/j.cclet.2022.04.015
1001-8417/

Traditional wastewater treatment technologies, such as biological degradation and physical adsorption methods, cannot achieve the efficient degradation of domestic and hospital effluents. Recently, microbial fuel cell (MFC) is employed to degrade various organic matter while simultaneously generating electricity [11–13]. In order to further promote the application of MFC, there is an urgent need to enlarge specific surface area of photoanode, improve biocompatibility and corrosion resistance as well as simplify the synthetic procedures and decrease the cost [14–16]. The advanced oxidation technology for the treatment of industrial wastewater become an important approach for organic pollutant treatment due to a significant removal effect of high concentration of organic pollutant [17–19]. In particular, photocatalysis process as a high-performance advanced oxidation process can degrade complex organic pollutants in wastewater in a relatively inexpensive and environmental-friendly manner. Theoretically speaking, water is the reaction product which does not generate any pollutant. Furthermore, photocatalytic fuel cell (PFC) can be developed as a sustainable technology for simultaneously achieving the removal of organic pollutants and generating electricity. Through the recovery of the chemical energy contained in organic pollutants, PFC is considered a green technology to convert organic wastes into electric energy, providing a potential solution to solve the environmental problem and energy crisis. Under light irradiation, the photogenerated holes can react with H_2O to produce hydroxyl radicals ($^{\bullet}OH$) on the photoanode while the photogenerated electrons react with O_2 to generate superoxide radicals ($^{\bullet}O_2^-$) at the cathode. The photogenerated holes are then consumed to degrade organic pollutants, such as antibiotics and dyes [20–22]. Nevertheless, previous studies revealed that the further development of PFCs is currently limited by their low performance due to the complexity of the fabrication and the poor separation and/or utilization of photogenerated electron-hole pairs [23]. Therefore, it is urgent to reduce the manufacturing cost and improve the utilization of photogenerated carriers in the PFC [24–27].

Among the existing photocatalytic materials, titanium dioxide (TiO_2) receives increasing attention because of its high chemical stability, low cost, non-toxicity and high photocatalytic activity [28,29]. However, pristine TiO_2 can only absorb ultraviolet (UV) light and thus have low utilization of sunlight. Additionally, the rapid recombination of photogenerated electron-hole pairs leads to a dramatical decrease in photodegradation efficiency, which is still a serious barrier that limits their photocatalytic performance [30]. Therefore, numerous efforts have been devoted to develop innovative strategies to enhance the photocatalytic performance of TiO_2. Recently, it has been reported that 3D layered TiO_2 self-assembled from 1D nanostructures possessed outstanding photocatalytic activity since the 1D nanostructures could effectively accelerate the transfer rate of electrons and suppress the recombination of electron-hole pairs, meanwhile, 3D hierarchical structures could enlarge the surface area and enhance the light harvesting capability of TiO_2 [31]. For example, Zhou *et al.* synthesized a 3D sea-urchin-like hierarchical TiO_2 microsphere structure with remarkable photocatalytic activity [32]; Sadhu *et al.* successfully prepared 3D rutile TiO_2 microspheres composed of 1D nanostructures with enhanced photoelectrochemical and photocatalytic properties in Rhodamine B degradation [33]. Towards promoting photocatalytic degradation efficiency, a significant increase in the specific surface area was considered one of the most effective ways providing more active sites. According to previous reports, TiO_2 powder-based catalysts were deposited on conductive transparent substrates through coating and/or depositing process, such as fluorine-doped tin oxide (FTO) or indium tin oxide (ITO) coated glass. However, the obvious shortcomings of this commonly used approach are that the poor mechanical stability and high internal resistance between the catalyst and conductive substrate. Furthermore, Ni foam with interlinked cellular structure, relatively high surface area and mechanical stability can be considered a highly promising conductive substrate for the design of binder-free photoanode [34].

TiO_2 nanoparticles were facilely fabricated on porous Ni foam as well, denoting as TiO_2-NPs@NF (more details can be found in Supporting information). The preparation flowchart was shown in Fig. S1 (Supporting information). An *in situ* growth method was used to grow TiO_2 onto Ni foam, which can effectively suppress the compounding of photogenerated electron-hole pairs. Avoid using adhesive to coat the FTO or other conductive electrodes, which will bring problems such as high internal resistance and adhesive shedding affecting water quality. The as-prepared samples were abbreviated as TiO_2-NPs@NF-*x*, where *x* denotes the adding amount of tetrabutyl titanate (*e.g.*, 10/20/30 mL). To further verify the influence of Ni foam on the material properties, the same synthetic method was conducted to fabricate TiO_2 nanoparticles on FTO (namely, TiO_2-NPs@FTO-20). The performance of these two photoanodes with different substrate were compared to evaluate the impact of substrate and promote the further development of PFC.

To investigate the crystal structure and composition, the as-synthesized TiO_2@NF-*x* samples were systemically examined by X-ray diffraction patterns (XRD) and X-ray photoelectron spectroscopy (XPS) respectively. Fig. 1a and Fig. S2 (Supporting information) exhibited the X-ray diffraction (XRD) spectra of TiO_2-NPs@NF-*x* ($x = 10$, 20 and 30) and TiO_2-NPs@FTO-20, confirming the successful loading of TiO_2 nanoparticles on porous Ni foam and FTO. The characteristic diffraction peaks can be identified at $2\theta = 43.8°$ corresponding to (111) planes of rutile-phase TiO_2. The characteristic diffraction peaks of anatase-phase TiO_2 can be clearly identified in the all as-fabricated samples, which can be identified at $2\theta = 25.3°$, 37.4° and 62.9°, corresponding to (101), (004) and (204) planes of TiO_2 (JCPDS No. 21-1272) [35]. It can be concluded that anatase was the dominant phase in both TiO_2-NPs@NF-*x* ($x = 10/20/30$) and TiO_2-NPs@FTO-20 samples. As shown in Fig. 1a, the sharp diffraction peaks indicated that TiO_2 was well crystallize. Besides, the peaks at 44.6°, 51.9° and 76.4° were ascribed to the Ni foam substrate [36]. To further study the composition and valence states of TiO_2-NPs@NF-*x*, XPS spectra of all as-obtained samples were shown in Figs.1b-e and Fig. S3 (Supporting information). In fact, the XPS full scan of TiO_2-NPs@NF-20 exhibited characteristic signals of Ni Ti, O in all samples and no other impurity peaks were observed. The characteristic signals at binding energy of 855.48 and 872.89 eV was assigned to Ni $2p_{3/2}$ and Ni $2p_{1/2}$ orbital due the deposition of anatase TiO_2 nanoparticles on porous Ni foam substrate (Fig. 1c) [37]. As shown in Fig. 1d, the Ti 2p spectrum of TiO_2-NPs@NF-20 can be deconvoluted into two peaks at 458.65 eV for Ti $2p_{3/2}$ and 464.37 eV for Ti $2p_{1/2}$, respectively, corresponding to the lattice Ti-O bond in TiO_2 [38]. Moreover, the XPS spectrum of O 1s can be deconvoluted into two characteristic peaks at 529.98 and 531.75 eV (Fig. 1e), corresponding to the Ti-O-Ti bonds (lattice O) and surface hydroxyl groups, respectively [39]. It should be noted that no peaks of nickel oxide were detected in all samples, confirming that the *in situ* growth of TiO_2 nanoparticles on the backbone of porous Ni foam. As presented in Fig. 1f, the UV–visible diffuse reflectance spectra (DRS) of TiO_2-NPs@FTO-20 and TiO_2-NPs@NF-*x* ($x = 10$, 20 and 30) were compared. It can be observed that the bandgap absorption onset was partially extended into the visible light region for TiO_2-NPs@FTO-20 and all TiO_2-NPs@NF-*x* samples. Among them, TiO_2-NPs@NF-20 demonstrated the strongest absorption in the range of 400–600 nm. According to previous reports, the optical bandgap of all photocatalysts was calculated based on the following Eq. 1 [40]:

$$\alpha h\gamma = A(h\gamma - E_g)^n \quad (1)$$

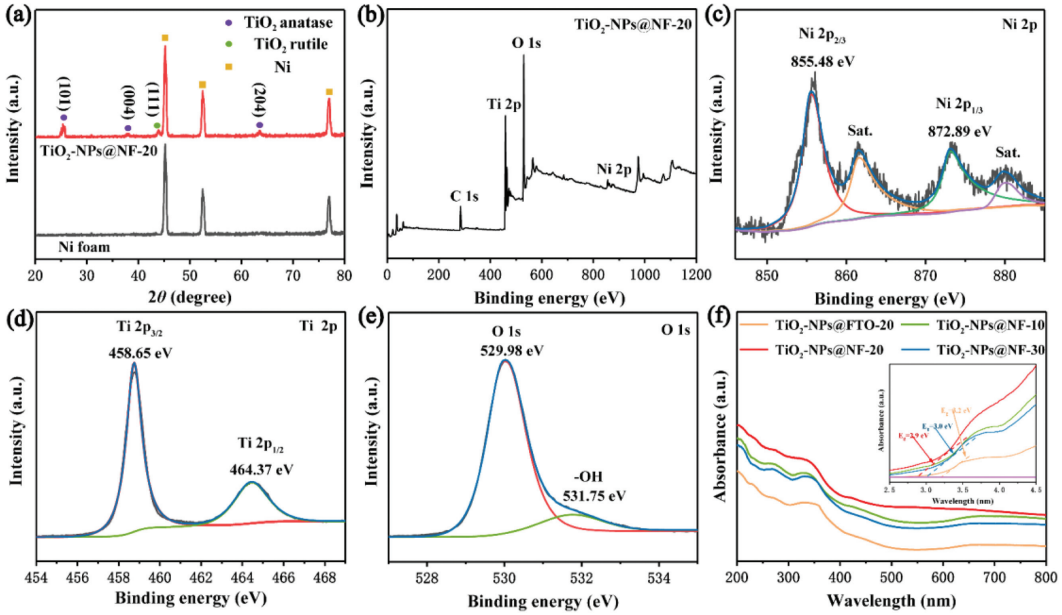

Fig. 1. (a) XRD patterns of Ni foam and TiO_2-NPs@NF-20. (b) XPS spectrum of the TiO_2-NPs@NF-20 composite. The high resolution XPS spectra for (c) Ni 2p, (d) Ti 2p and (e) O 1s, respectively. (f) UV–vis diffuse reflectance spectra and corresponding Kubelka-Munk plots (inset) of TiO_2-NPs@FTO-20, TiO_2-NPs@NF-10, TiO_2-NPs@NF-20 and TiO_2-NPs@NF-30 samples.

where α is the absorption coefficient, h is Planck's constant (4.136×10^{-15} eV s), γ is the light frequency (s^{-1}), A is an absorption constant, E_g is the band gap, n is assumed to be 1/2 and 2 for direct and indirect transitions, respectively [41]. As demonstrated in Fig. 1f, the Tauc plots indicated that the E_g value of TiO_2-NPs@NF-20 was calculated to be 2.9 eV. The E_g value of TiO_2-NPs@FTO-20 were calculated to be about 3.2 eV. In principle, the interlinked cellular structure of Ni foam can provide more sites for the growth of TiO_2 nanoparticles, which in turn improves light utilization.

The morphological characterization of TiO_2-NPs@NF-20 was presented in Fig. 2 and Fig. S4 (Supporting information). It can be clearly identified that TiO_2 NPs were grown uniformly on the porous Ni foam substrate in the precursors with 20 mL of tetrabutyl titanate. TiO_2-NPs@NF-20 inherited the ordered structural features of 3D materials, which facilitates photocarrier migration [42]. SEM images of as-fabricated photoanodes with higher magnifications were shown in Fig. S5 (Supporting information). The surface morphology of as-synthesized samples was found to vary considerably. Compared to the smoother and granulated surface of TiO_2-NPs@NF-20 (Fig. S5b), TiO_2-NPs@NF-10 (Fig. S5a) composites exhibit a delaminated and significantly roughened surface while spherical particles can be observed in TiO_2-NPs@NF-30 sample (Fig. S5c). As shown in Fig. S6 (Supporting information), EDX characterization further confirmed that the chemical composition of Ti, O and Ni in the TiO_2-NPs@NF-20 electrode, respectively. As shown in Figs. 2c and d, TEM characterization exhibited that TiO_2 NPs with average particle size about 20 nm were prepared.

Furthermore, transient photocurrent response and electrochemical impedance (EIS) measurements were conducted to evaluate photogenerated charge carrier separation efficiency and interfacial charge-transfer resistance, respectively. Fig. 3a demonstrated the typical photocurrent response of TiO_2-NPs@NF-x and TiO_2-NPs@FTO-20 with light on-off cycles. The photocurrent intensity

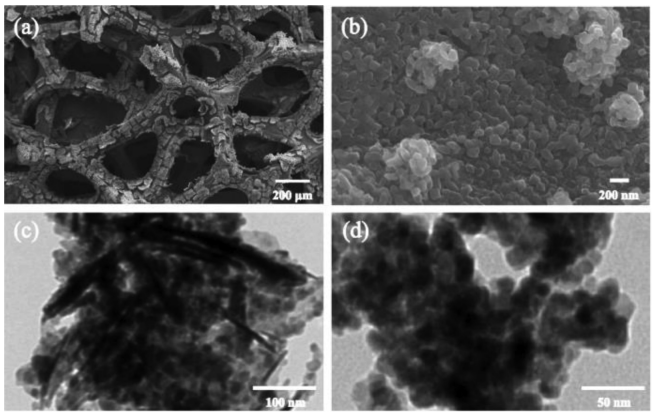

Fig. 2. (a, b) SEM images of TiO_2-NPs@NF-20 composite, (c, d) TEM images of TiO_2-NPs@NF-20 composite.

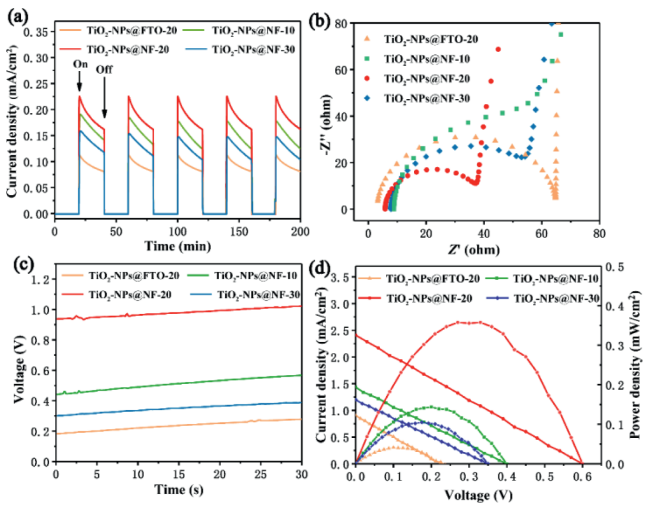

Fig. 3. (a) Transient photocurrent responses, (b) Nyquist plots of TiO_2-NPs@FTO-20, TiO_2-NPs@NF-10, TiO_2-NPs@NF-20 and TiO_2-NPs@NF-30 photoanodes. (c) Open circuit voltage, (d) *J-V* characteristic and power density of different photoanodes.

of TiO_2-NPs@NF-20 foam was much higher than the other samples, indicating a higher charge separation and migration efficiency and lower recombination probability of electron-hole pairs [43]. This may be due to the superior electrical conductivity of Ni foam. In addition, the photocurrent intensity was not suppressed with the prolongation of the reaction time, indicating that TiO_2-NPs@NF-*x* and TiO_2-NPs@FTO-20 can also facilitate a stable photoelectric activity. As shown in Fig. 3b, the EIS measurements were performed to explore their charge transfer property. The Nyquist plots confirmed that TiO_2-NPs@NF-20 processed a lower charge transfer resistance, indicating its fast interfacial charge transfer performance [44]. In order to evaluate their photoelectric performance, the as-fabricated PFC with the photoanode of TiO_2-NPs@NF-*x* and TiO_2-NPs@FTO-20 was tested in CIP-HCl. As presented in Figs. 3c and d, TiO_2-NPs@NF-20 exhibited the best performance with an open circuit voltage of 1.021 V and short circuit current density of 2.4 mA/cm^2 and maximum output power density of 0.357 mW/cm^2, respectively. It should be highlighted that TiO_2-NPs@NF-20 photoanode achieved the highest electricity production efficiency (Table S1 in Supporting information) among all PFC system due to the formation of highly ordered nanoparticles network which was assembled by consecutive deposition on highly conductive and porous Ni foam substrate. In the PFC system, TiO_2-NPs@NF-*x* photoanode served as a pivotal role to generate electron-hole pairs by photoexcitation to promote electrical energy output.

The photocatalytic degradation performance of different TiO_2-NPs@NF-*x* and TiO_2-NPs@FTO-20 was assessed by using CIP-HCl as the target pollutant in a short period of time, TiO_2-NPs@FTO-20 and TiO_2-NPs@NF-*x* as the photoanode and Pt as the cathode to form a PFC system. As shown in Fig. 4a, the antibiotic degradation efficiencies were investigated for TiO_2-NPs@FTO-20 and TiO_2-NPs@NF-*x* samples after 3 h light illumination. It can be concluded that CIP-HCl cannot be degraded under light irradiation. The TiO_2-NPs@FTO-20 can degrade 50% of CIP-HCl. The degradation efficiency of TiO_2-NPs@NF-20 photoanode (85%) was higher than other TiO_2-NPs@NF-*x* ($x = 10/30$). The kinetic rates for the degradation of CIP-HCl was shown in Fig. S7a (Supporting information), which are in accordance with *pseudo*-first-order kinetic equation. Fig. S7b (Supporting information) demonstrated the absorbance spectra of photocatalytic degradation of CIP under Xe lamp irradiation as a function of reaction time. Combined with the results of the photovoltaic performance test, it can be concluded that the optimal amount of tetrabutyl titanate is 20 mL, and TiO_2 can be uniformly grown on Ni foam. To investigate whether the as-fabricated photocathode can further degrade CIP-HCl over a longer period of time, we conducted photocatalytic experiment with 6 h by using TiO_2-NPs@NF-20 as photoanode, and 95% of CIP was removed after 6 h (Fig. S7c in Supporting information). However, the degradation of CIP-HCl was found to be insufficient at less than 3 h. Therefore, the subsequent experiments were carried out for 3 h as the experimental period. The Ni foam was employed to provide more active sites for the growth of TiO_2 nanoparticles, and improve the utilization of light. Using Ni foam as photoanode substrate can effectively promote the generation and separation of photogenerated electron-hole pairs and enhance the PFC performance. With a large short-circuit current and high oxidation ability, PFC could offer a great potential for pollutants elimination and simultaneous electricity generation with high efficiency.

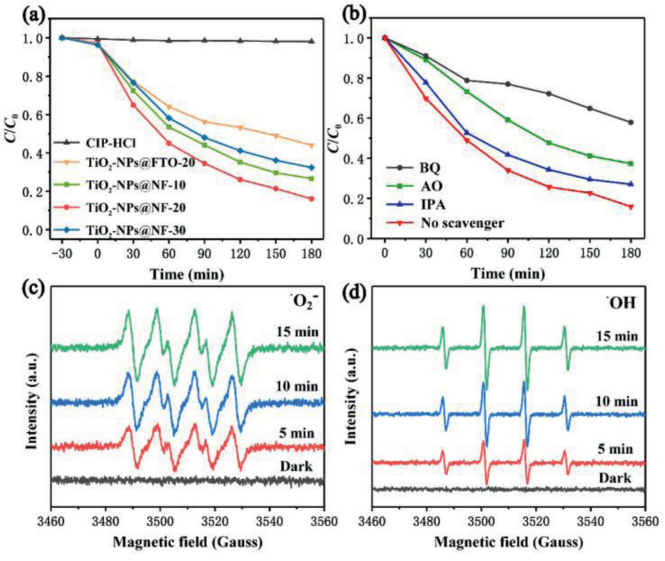

Fig. 4. (a) Plot of C/C_0 *versus* time for degradation of CIP-HCl during the photocatalytic processes. (b) Degradation of CIP-HCl in photocatalysis with TiO_2-NPs@NF-20 alone, and contrast that with BQ, AO and IPA adding in the system. ESR spectra of TiO_2-NPs@NF-20 in aqueous solution before and after light irradiation: (c) DMPO-$^{\bullet}O_2^-$ and (d) DMPO-$^{\bullet}$OH.

Influences of initial CIP-HCl concentration and solution pH on photocatalytic performance were tested to optimize the PFC performance. In order to optimize the photoanode performance, we explored the efficiency of TiO_2-NPs@NF-20 foam in degrading CIP-HCl at different pH condition. CIP-HCl solution was generally neutral and pH is generally 6.9. In this work, pH 3 and 11 was chosen as the acid and alkaline conditions to investigate the optimal performance conditions for the PFC system. As depicted in Figs. S8a and b (Supporting information), the removal of CIP-HCl at initial pH 3,7,11 was found to be 35%, 85%, and 63%, respectively. CIP-HCl can be efficiently removed under neutral conditions, which would be suitable for most practical wastewater. The highest degradation rates were observed for zwitterionic form of CIP [45]. The removal efficiency of CIP was found to be quite low under acidic and alkaline conditions mainly due to the decreased electrostatic interaction between the photocatalyst and the contaminant. Under acidic conditions, ciprofloxacin exhibited positive surface charges [46] while TiO_2 were found to be positive as well. Under alkaline conditions, ciprofloxacin showed surface charges [46] but TiO_2 also carried negative surface charges. Therefore, the electrostatic repulsion existed between them, which lower the removal efficiency of ciprofloxacin. However, under neutral conditions, the electrostatic interaction between TiO_2 NPs and ciprofloxacin facilitate the removal of ciprofloxacin.

Figs. S8c and d (Supporting information) presented the influence of initial CIP-HCl concentration on the photocatalytic performance using CIP-HCl under neutral conditions. The experimental results indicated that the reactions were consistent with the first-order kinetic mode. It should be noted that the photocatalytic performance was found to be worse when further increasing the CIP-HCl concentrations above 30 mg/L. It can be ascribed to the insufficient active sites available on TiO_2-NPs@NF-20 photoanode for CIP-HCl degradation at very high concentrations. In fact, the adsorption of the CIP on the TiO_2-NPs@NF-20 surface might be then halted [47]. When the concentration of CIP-HCl was relatively small, there was no significant difference in the removal rate, indicating the efficient removal of trace organic pollutants in water.

The sustainability of photoanode was one of the key factors limiting the practical applications of PFC. The recyclability of the PFC system was investigated by continuous treatment of the solution containing 1, 10, 30 mg/L of CIP-HCl under optimized conditions. Fig. S9 (Supporting information) showed the removal of CIP-HCl by the established PFC system for 5 cycles. With increasing of the numbers of runs, TiO_2-NPs@NF-20 photoanode remained relatively stable after durability test. The CIP-HCl removal rate did not decrease significantly, the mass loss rate of the photoanode was

about 5% (Table S2 in Supporting information), confirming the high stability and recyclability of the as-fabricated PFC system for long-time applications. It can be concluded that the developed PFC system not only had high photoelectric activity, but also showed good stability. The slow decay in the treatment performance of the proposed PFC system might be due to the adsorption of some intermediates on the photoanode surface, which slightly prevented the direct transfer of photogenerated charges from the photocatalyst to the substrate [48,49].

At the optimum 10 mg/L initial CIP-HCl concentration and solution pH of 7, the roles of four different quenchers, namely *p*-benzoquinone (BQ) for superoxide ion ($^{\bullet}O_2^-$), ammonium oxalate (AO) for photogenerated holes (h^+), and isopropanol (IPA) for hydroxyl radical ($^{\bullet}OH$) were investigated according to previously reported methods [50,51]. As shown in Fig. 4b, the CIP-HCl removal efficiency in the PFC achieved at 85% without any quenchers. When the 1 mmol/L BQ were added, the CIP-HCl removal was found to be strongly suppressed to 42%. However, the addition of AO and IPA had less effect on the CIP-HCl removal (62.6% and 73%, respectively). Thus, the degradation efficiency of the active species could be given in the following order: $^{\bullet}O_2^- > h^+ > {}^{\bullet}OH$. To further investigate on the aforementioned radicals, ESR technique was also employed with DMPO as a spin trap and the results are disclosed in the inset of Figs. 4c and d. Generally, no signals could be observed for both $^{\bullet}OH$ and $^{\bullet}O_2^-$ under dark condition. It can be seen that the 4-fold characteristic peak with an intensity ratio of 1:1:1:1 for DMPO-$^{\bullet}O_2^-$ was observed in the PFC system [52]. In addition, the characteristic signals with 1:2:2:1 was identified as the DMPO-$^{\bullet}OH$ signal peak [53]. With the increase of the light time, the peak was getting larger and larger, indicating the ability of TiO_2-NPs@NF-20 to generate $^{\bullet}O_2^-$ and $^{\bullet}OH$ radicals under light irradiation. These results were in accordance with the outcomes of radical trapping experiments. The mechanism of this PFC system (Fig. S10 in Supporting information) to degraded the CIP-HCl and simultaneous power generation can be speculated as under irradiation, TiO_2-NPs@NF-20 (band gap energy 2.9 eV) can absorb light efficiently under the light illumination, and the ordered growth of TiO_2 generates more photogenerated carriers and electrons (e^-) will be excited at the conduction band (CB). Due to the excellent electrical conductivity of Ni foam, electrons tended to transfer to the Pt electrode through Ni foam, and the electrical generation performance was more outstanding. The electrons reacted with oxygen at the cathode to generate superoxide ions. The remaining parts were holes (h^+) with strong oxidation ability at the valance band (VB). The photo-generated holes reacted with water and OH^- to form $^{\bullet}OH$. Both holes and $^{\bullet}OH$ were oxidizing, and these reactive groups were involved in the CIP-HCl degradation process. The outstanding electrical conductivity of Ni foam increased the rate of electron transfer, which generated more $^{\bullet}O_2^-$ and leads to $^{\bullet}O_2^-$ as the main reactive species.

In conclusion, TiO_2-NPs@NF-20 with interlinked cellular structure was synthesized by a cost-efficient hydrothermal method and developed as photoanode for enhanced organic pollutants degradation and electricity generation. In comparison with TiO_2-NPs@FTO-20 and other TiO_2-NPs@NF-*x* ($x = 10/30$) photoanode, TiO_2-NPs@NF-20 demonstrated excellent electrical conductivity, facilitating the separation of photogenerated carriers and accelerating their degradation rate. In this work, a degradation ability for CIP-HCl with a removal efficiency of 85% was achieved with short-circuit current density and maximum power density of 2.4 mA/cm^2, 0.357 mW/cm^2, respectively. Compared to previous reports (Table S3 in Supporting information), the PFC with TiO_2-NPs@NF-20 as photoanode and Pt as cathode shows high performance of organics to electricity under light irradiation. Moreover, the good electrical conductivity of Ni foam can considerably enlarge the surface area and promote the transport of photogenerated carriers, which played an essential in boosting the photocatalytic activity of TiO_2 nanoparticles. After 5 cycles, the removal rate of CIP-HCl was still found to be 85%, indicating the TiO_2 nanoparticles decorated Ni foam as a robust photoanode of PFC system was suitable to develop as a platform for simultaneous energy generation and wastewater treatment. This type of PFC also demonstrated excellent removal rates for other organic dyes (Fig. S11 in Supporting information). In the future, several reactor units will be designed in series to circulate the wastewater, aiming at creating a highly-efficient and stable small PFC unit and laying a good foundation for the wide application of PFC in wastewater remediation.

Declaration of competing interest

We declare that we have no known competing financial interests or personal relationships that could have appeared to influence the work reported in this paper.

Acknowledgments

This research was funded by the National Science and Technology Major Project for Water Pollution Control and Treatment (No. 2018ZX07110-008), National Natural Science Foundation of China (No. 21777065), Basic Scientific Re-search Business Expense Project of Beijing University of Civil Engineering and Architecture (No. X18005) and the 2021 BUCEA Post Graduate Innovation Project.

Supplementary materials

Supplementary material associated with this article can be found, in the online version, at doi:10.1016/j.cclet.2022.04.015.

References

[1] Q.Q. Zhang, G.G. Ying, C.G. Pan, et al., Environ. Sci. Technol. 49 (2015) 6772–6782.
[2] M. Malakootian, A. Nasiri, M.A. Gharaghani, Chem. Eng. Commun. 207 (2020) 56–72.
[3] K.R. Kelly, B.W. Brooks, Prog. Mol. Biol. Transl. 159 (2018) 59–77.
[4] N. Liu, N. Lu, Y. Su, et al., Sep. Purif. Technol. 211 (2019) 782–789.
[5] L.J.M. Githinji, M.K. Musey, R.O. Ankumah, Water, Air, Soil Pollut. 219 (2011) 191–201.
[6] J.Q. Jiang, Z. Zhou, O. Pahl, Sep. Purif. Technol. 88 (2012) 95–98.
[7] E.C. Dogan, Global NEST J. 18 (2016) 291–308.
[8] X.H. Wang, A.Y.C. Lin, Environ. Pollut. 186 (2014) 203–215.
[9] O. Fasugba, A. Gardner, B.G. Mitchell, et al., BMC Infect. Dis. 25 (2015) 545.
[10] A.K. Venkatesan, R.U. Halden, Sci. Rep. 4 (2014) 03731.
[11] B.E. Logan, B. Hamelers, R. Rozendal, et al., Environ. Sci. Technol. 40 (2006) 5181–5192.
[12] D.R. Lovley, Curr. Opin. Biotechnol. 19 (2008) 564–571.
[13] B.E. Logan, R. Korneel, Science 337 (2012) 686–690.
[14] W.W. Li, H.Q. Yu, Z. He, Environ. Sci. Technol. 7 (2014) 911–924.
[15] B.E. Logan, M.J. Wallack, K. Kim, et al., Environ. Sci. Technol. Lett. 2 (2015) 206–214.
[16] H.Y. Yuan, Z. He, Nanoscale 7 (2015) 7022–7029.
[17] A. Buthiyappan, A.A.A. Raman, J. Clean. Prod. 206 (2019) 1025–1040.
[18] J. Wang, C. Liu, J. Feng, et al., J. Hazard. Mater. 394 (2020) 122567.
[19] J. Lu, Y. Zhou, J. Lei, et al., Chemosphere 251 (2020) 126402.
[20] M.H. Li, Y.B. Liu, L.M. Dong, et al., Sci. Total Environ. 668 (2019) 966–978.
[21] P.R. Ding, H.D. Hao, P.S. Li, et al., Appl. Catal. B: Environ. 300 (2022) 120633.
[22] X. Wang, W.Y. Lu, Z.G. Zhao, et al., Chem. Eng. J. 400 (2020) 125872.
[23] T. Parvizi, J.B. Parsa, R. Farnood, et al., Electrochim. Acta 370 (2021) 13773.
[24] G. Liu, G.P. Jiang, M. Fowler, et al., J. Power Sources 425 (2019) 69–75.
[25] M.J. Munoz-Batista, G.R. Bertolini, C.I. Cabello, et al., Appl. Catal. B 238 (2018) 381–392.
[26] K. Ouyang, S. Xie, P. Wang, et al., Int. J. Hydrogen Energy 44 (2019) 7288–7299.
[27] Y. He, R.H. Yuan, M.K.H. Leung, Mater. Lett. 236 (2019) 394–397.
[28] Y.N. Tang, H. Sun, Y.X. Shang, et al., J. Colloid Interface Sci. 535 (2019) 516–523.
[29] Y. Ma, X. Wang, Y. Jia, et al., Chem. Rev. 114 (2014) 9987–10043.
[30] Z.J. Li, Y. Wang, A.A. Elzatahry, et al., Chin. Chem. Lett. 31 (2020) 1598–1602.
[31] S.P. Xu, X. Sun, Y. Zhao, et al., Appl. Surf. Sci. 448 (2018) 78–87.
[32] Y. Zhou, Y. Wang, Q. Yi, et al., J. Mater. Sci.-Mater. Electron. 25 (2014) 4156–4162.
[33] S. Sadhu, P. Gupta, P. Poddar, ACS Appl. Mater. Interfaces 9 (2017) 11202–11211.
[34] Y. Zhang, M.T. Shi, C.Z. Wang, et al., Sci. Bull. 65 (2020) 359–366.
[35] L. Ding, S.R. Yang, Z.Q. Liang, et al., J. Colloid Interface Sci. 567 (2020) 181–189.

[36] R.Q. Yang, Y.C. Ji, J. Zhang, et al., Catal. Today 335 (2019) 520–526.
[37] I. Abidat, C. Morais, C. Comminges, et al., J. Mater. Chem. A 15 (2017) 7173–7183.
[38] L.X. Zheng, S.C. Han, H. Liu, et al., Small 12 (2016) 1527–1536.
[39] A. Mirzaei, Z. Chen, F. Haghighat, et al., Chemosphere 205 (2018) 463–474.
[40] A. Kumar, A. Kumar, G. Sharma, et al., Chem. Eng. J. 334 (2018) 462–478.
[41] A. Kumar, A. Kumar, G. Sharma, et al., J. Clean. Prod. 165 (2017) 431–451.
[42] J.H. Wang, Y.F. Shen, S.Q. Liu, et al., Appl. Catal. B: Environ. 270 (2020) 118885.
[43] S.M. Lam, J.C. Sin, H.H. Zeng, et al., Sep. Purif. Technol. 265 (2021) 118495.
[44] D. Zhang, Y.M. Wang, Y. Wang, et al., J. Alloys Compd. 815 (2020) 152377.
[45] S. Li, T.B. Huang, P.H. Du, et al., Water Res. 185 (2020) 116286.
[46] S.P. Sun, T.A. Hatton, T.S. Chung, Environ. Sci. Technol. 45 (2011) 4003–4009.
[47] P. Martins, S. Kappert, H.N. Le, et al., Catalysts 10 (2020) 234–253.
[48] Q. Sun, S.H. Wu, D. You, et al., Appl. Surf. Sci. 467-468 (2019) 825–835.
[49] Q.Y. Zeng, L. Lya, Y.W. Gao, et al., Appl. Catal. B: Environ. 238 (2018) 309–317.
[50] D.Q. Gao, Y.G. Liu, P. Liu, Sci. Rep. 6 (2016) 35768-35755.
[51] Y.X. Wang, F.T. He, C. Lin, et al., Chin. Chem. Lett. 31 (2020) 2668–2672.
[52] S. Chen, Y. Hu, S. Meng, et al., Appl. Catal. B: Environ. 150 (2014) 564–573.
[53] W. Qin, G. Fang, Y. Wang, et al., Chem. Eng. J. 348 (2018) 526–534.